Theoretical and experimental investigations of Coulomb blockade in coupled quantum dot systems

Franz J. Kaiser, Sigmund Kohler, Peter Hänggi, Marcin Malecha, Jens Ebbecke, Achim Wixforth, H. W. Schumacher, B. Kästner, Daniel Reuter, Andreas D. Wieck

Angaben zur Veröffentlichung / Publication details:

Kaiser, Franz J., Sigmund Kohler, Peter Hänggi, Marcin Malecha, Jens Ebbecke, Achim Wixforth, H. W. Schumacher, B. Kästner, Daniel Reuter, and Andreas D. Wieck. 2008. "Theoretical and experimental investigations of Coulomb blockade in coupled quantum dot systems." *Journal of Physics: Condensed Matter* 20 (37): 374108. https://doi.org/10.1088/0953-8984/20/37/374108.

Theoretical and experimental investigations of Coulomb blockade in coupled quantum dot systems

F J Kaiser[1], S Kohler[1], P Hänggi[1], M Malecha[2], J Ebbecke[2], A Wixforth[2], H W Schumacher[3], B Kästner[3], D Reuter[4] and A D Wieck[4]

[1] Theoretische Physik I, Institut für Physik der Universität Augsburg, Universitätsstraße 1, 86135 Augsburg, Germany
[2] Experimentalphysik I, Institut für Physik der Universität Augsburg, Universitätsstraße 1, 86135 Augsburg, Germany
[3] Physikalisch-Technische Bundesanstalt, Bundesallee 100, D-38116 Braunschweig, Germany
[4] Angewandte Festkörperphysik, Ruhr-Universität Bochum, 44780 Bochum, Germany

E-mail: franz.josef.kaiser@physik.uni-augsburg.de

Abstract
Two strongly coupled quantum dots are theoretically and experimentally investigated. In conductance measurements on a GaAs based low-dimensional system additional features to the Coulomb blockade have been detected at low temperatures. These regions of finite conductivity are compared with theoretical investigations of a strongly coupled quantum dot system and good agreement between the theoretical and the experimental results has been found.

(Some figures in this article are in colour only in the electronic version)

1. Introduction

Electron transport through a single quantum dot in a two-terminal configuration is governed by the interaction energy of the electrons on the dot. In many experiments, the state of the quantum dot is essentially characterized by the electron number, since orbital degrees of freedom do not play a major role and can thus be ignored. In the limit of weak dot–lead coupling, the resulting current is determined by states with an energy above the Fermi energy of one lead but below the Fermi energy of the other lead. The other states suffer Coulomb blockade: energy conservation together with Pauli's exclusion principle preserves their occupation number and, consequently, they cannot contribute to the transport. Only when the dot–lead coupling becomes larger do co-tunnelling processes start to play a role and suspend Coulomb blockade.

When two or more quantum dots are in a linear transport arrangement between two leads, the inter-dot tunnelling can be incoherent or coherent, depending on the coupling strength. Incoherent tunnelling is sequential, i.e. between two tunnelling events, the electrons dwell in one particular dot. Coherent tunnelling is found for strong inter-dot coupling such that the electrons reside in the delocalized eigenstates of the double dot. The analogy to π-electrons in molecules is reflected by the term 'artificial molecule'. A convenient theoretical picture for coherently coupled quantum dots is of one single central system in which orbital degrees of freedom play a role.

In an unbiased double dot, the relevant orbitals are the bonding and the anti-bonding superposition of the localized states. Then an electron prepared in one dot will tunnel back and forth to the other dot with a frequency set by the tunnel splitting. These coherent oscillations can be observed by lowering, after a waiting time, the chemical potential of, say, the right lead. If at that stage the electron is in the right dot it will tunnel to the right lead. Periodic repetition of this procedure yields a dc current that reflects the coherent oscillations [1]. The coherence of the superposition together with the possibility of performing a readout allows one to devise charge qubits with double quantum dots. The orbital degrees also influence the transport under microwave excitation: microwave irradiation can induce electron transitions from the ground state to an excited state

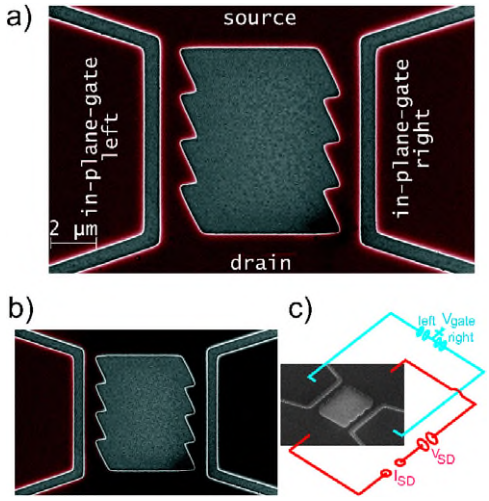

Figure 1. (a) Scanning electron micrograph of the sample. Red (darker) areas are highlighting 2DEG, grey (brighter) areas are wet-etched and non-conducting. The annealed ohmic contacts (not shown) are labelled. The depletion of the left channel (under investigation) is controlled by the left in-plane gate. The channel can be made narrower by applying a more negative voltage to the gate until all electrons are forced out of the channel. In our experiment the right channel is completely depleted by applying a sufficiently large voltage (-4.5 V) to the right gate as shown in panel (b). (c) Wiring scheme of the sample.

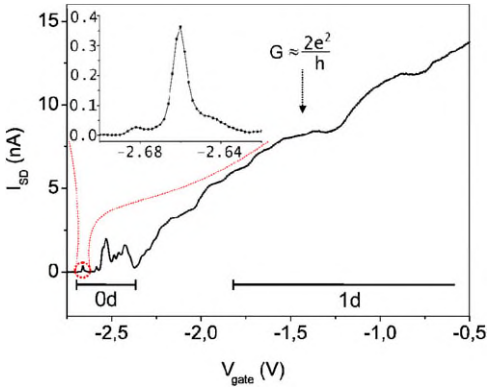

Figure 2. Measured current through the left channel with decreasing voltage on the left in-plane gate at 1.3 K. The applied source–drain voltage is $V_{SD} = 0.1$ mV. The system is evolving from the 1D regime, characterized by current plateaus, into the QD regime with characteristic Coulomb oscillations. Inset: blow-up of the very first oscillation ($V_{gate} = -2.66$ V) next to the pinch-off.

and thereby enhance the electron transport between the leads, so that one observes photon-assisted tunnelling [2–4].

A further common method for characterizing low-dimensional semiconductor systems such as the mentioned quantum dots is conductance measurements at low temperature: since the current changes whenever an energy level enters or leaves the voltage window, the differential conductance exhibits a corresponding peak. Shifting, in addition, the energy levels by a gate voltage yields the characteristic 'Coulomb diamonds' which are observed in the differential conductance as a function of gate voltage and bias voltage. Within this work, we study both theoretically and experimentally the fingerprints of orbital degrees of freedom in the Coulomb diamond structure of coherently coupled quantum dots. In section 2 we describe our experimental setup and present transport measurements, while in section 3 we study a minimal model that exhibits the observed Coulomb diamonds. Moreover, we relate our theoretical findings to the experimental data.

2. Experimental setup

In this work we used a GaAs/AlGaAs heterostructure for sample fabrication, where the two-dimensional electron gas (2DEG) is located approximately 55 nm beneath the sample surface [5]. First, a mesa structure was defined by photolithography, followed by wet-etching and annealing of ohmic contacts for source, drain and in-plane gates. Then the nanostructure formation was processed by electron beam lithography and wet-etching [6]. Figure 1 shows the nanostructure under investigation. While the grey (light) areas were etched, the red (dark) areas depict the regions containing a high mobility 2DEG. The structure is 8 μm long and in total about 10 μm wide. The inner structure is sawtooth shaped with four teeth and asymmetric with respect to the vertical centre line. The conductive channels between the sawtooth-tip and in-plane gates are approx. 0.9 μm wide. The 2DEG has an electron density of 3.95×10^{15} μm^{-2} and a mobility of 51.7 m^2 V^{-1} s^{-1} (both measured in the dark at $T = 4.2$ K). The sample allows us to carry out measurements individually on each channel. Here, we report only on measurements on the left channel. In order to ensure that only the left channel is conductive and the measurement is not affected by the right channel, a relatively high negative voltage of -4.5 V is applied to the right in-plane gate. This causes a depletion [7, 8] of the 2DEG in the right channel such that no electrons can pass from source to drain. This situation is shown in figure 1(b), while figure 1(c) sketches the wiring scheme of the sample. In the same manner, the left channel can be depleted as well. If a negative gate voltage is applied, the channel becomes narrower until three potential barriers between the depleted areas, developed from the voltage on the gate and the wet-etched tines, are formed. Now, the 1D channel is separated into shorter channels and with decreasing gate voltage it eventually evolves into small quantum dots. At a certain voltage, the so-called pinch-off, the channel is completely depleted and, consequently, no current can flow. Such an evolution from a one-dimensional (1D) channel [9, 10] over quantum dots (QD) [10–14] to total depletion is shown in figure 2. At less negative gate voltages, characteristic 1D conductance quantization in the form of current steps—conduction plateaus—can be seen. At even more negative voltages current oscillations were observed, being characteristic for QD transport. The irregularity of the current peaks as a function of the side gate voltage already indicates the existence of a rather complicated electronic structure close to the pinch-off. The measurement in figure 2 was carried out at temperature $T = 1.3$ K with a source–drain bias voltage $V_{SD} = 0.1$ mV.

Because it is quite difficult to estimate the exact landscape of the barriers and to explain the measurements in greater

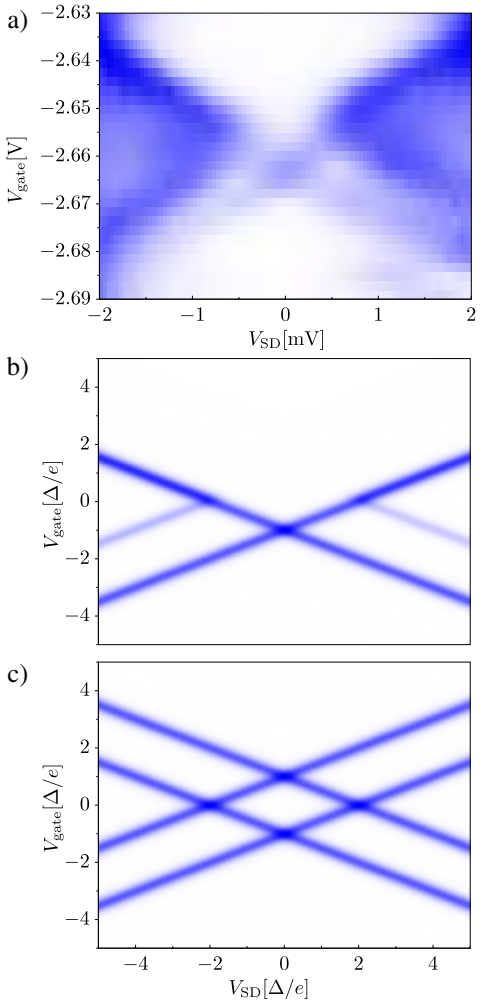

Figure 3. False colour plot of the differential conductance $\mathrm{d}I/\mathrm{d}V_{\rm SD}$ as a function of source–drain bias and gate voltage. Bright corresponds to low conductance and blue to high conductance. The experimental data (a) described in section 2 are compared to theoretical results for a double quantum dot with interacting (b) and non-interacting (c) electrons. The theoretical calculations are for dot–lead couplings $\Gamma_{\rm L} = 0.2\Delta$, $\Gamma_{\rm R} = 0.25\Delta$ and temperature $T = 0.1\Delta/k_{\rm B}$.

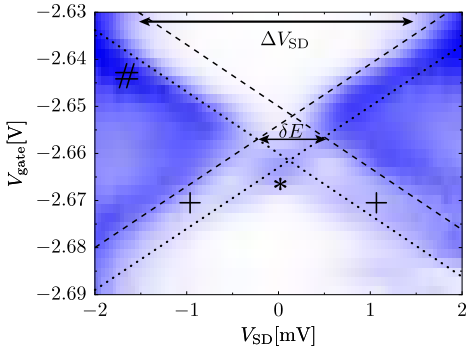

Figure 4. Sketch of the system characteristics superimposed on the experimental data. From the slope of the dashed lines one can estimate the capacities of the dot; the dotted lines highlight the stripes of elevated conductivity. The symbols $*$, $+$ and # mark parameter regions mentioned in the text. The total capacity of the system, C_Σ, can be estimated from the value of $\Delta V_{\rm SD}$ [15].

detail if the channel consists of more than one QD, we focused on measurements very close to the pinch-off, where the first current oscillation appears. The first current peak is at $V_{\rm gate} = -2.66$ V (see inset of figure 2). This quantum dot system can be characterized by a set of current measurements for different source–drain voltages [15]. Figure 3 shows the corresponding differential conductance $\mathrm{d}I/\mathrm{d}V_{\rm SD}$ which exhibit a characteristic Coulomb diamond structure [11–13, 15]. From the slopes of the transition from high to low conductivity shown in figure 4, one can extract the effective parameters which we use later in our theoretical description [15]: the capacities $C_{\rm gate} = (4 \pm 1) \times 10^{-18}$ F, $C_{\rm drain} = (51 \pm 15) \times 10^{-18}$ F and $C_\Sigma = (103 \pm 8) \times 10^{-18}$ F where $C_{\rm gate}$ is the capacity between the dot and the gate, $C_{\rm drain}$ the dot–drain capacity and C_Σ the total dot capacity. The single electron charging energy is $E_{\rm C} = 0.78 \pm 0.06$ meV and the energy spacing between two levels inside the dot is $\Delta E = 1.6 \pm 0.1$ meV. The relatively large uncertainties follow from the estimated uncertainty of reading the quantities from figure 3 and from the calculated propagation of uncertainty. If one assumes a parabolic potential, the energy spacing lets us estimate the lateral dimension of $(14 \pm 1) \times 10^{-15}$ m^2 of the dot and the diameter of (136 ± 6) nm. However, because of the triangular shape from the lithographically defined sawtooth potential, it is unlikely that the dot is perfectly round and a irregular shape is assumed.

Figure 3(a) shows the differential conductance $\mathrm{d}I/\mathrm{d}V_{\rm SD}$. It exhibits some differences from 'regular' Coulomb diamonds. First, the diamond is slightly tilted to the left. This is an indication for asymmetric tunnelling barriers between the QD and the leads as seen in almost every Coulomb diamond measurement. Second, some additional structures in the diamond can be spotted. The most obvious one is the small area of high conductivity in the centre section where the tips of conductive areas almost merge (marked with $*$ in figure 4). A further interesting feature is the narrow stripes of finite conductance alongside the main areas (marked with $+$). These mentioned areas are also rather symmetric due to bias source–drain voltage and asymmetric along the gate voltage, i.e. they appear only for lower gate voltages whereas the transition from electron transport to Coulomb blockade for higher gate voltages is very sharp. The third area (marked with #) exhibits a high conductivity and is also symmetric in the source–drain voltage but not as a function of the gate voltage.

3. Theoretical description

For a master equation description of electron transport at very low bias voltages one needs to take particular care to avoid inconsistencies like the emergence of spurious non-vanishing transport in equilibrium situations. Such problems typically arise from the approximation in the interaction representation of the coupling operator [4, 16]. A detailed derivation of such a master equation approach has been presented in [17], for example. Here, we will briefly review this approach.

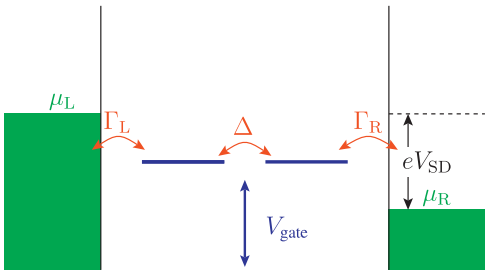

Figure 5. Tight-binding model for a double QD coupled to two leads. An external bias voltage $V = (\mu_R - \mu_L)/e$ is applied to the mesoscopic system.

3.1. Model

The setup at hand for studying coherent quantum transport is shown in figure 5 and the corresponding Hamiltonian reads

$$H = H_{\text{dots}} + H_{\text{leads}} + H_{\text{dots-lead}}. \tag{1}$$

The individual terms describe the QDs, the electron reservoirs of the leads and the coupling of the dots to the leads. The system itself is treated in a tight-binding approximation which we restrict in the following to two orbital degrees of freedom. Since we aim at exploring blocking effects, the corresponding wire Hamiltonian, incorporating the Coulomb repulsion in the limit of a large interaction strength U, assumes the form

$$H_{\text{dots}} = \sum_n E_n c_n^\dagger c_n - \Delta\left(c_2^\dagger c_1 + c_1^\dagger c_2\right) + \frac{U}{2}\mathcal{N}(\mathcal{N}-1). \tag{2}$$

The fermion operators $c_n^\dagger$ (c_n) create (annihilate) an electron in the orbital $|n\rangle$, $n = 1, 2$, and E_n denotes the respective on-site energy. In the Coulomb interaction term, $\mathcal{N} = \sum_n c_n^\dagger c_n$ is the operator counting the excess electrons on the dots. The inter-dot coupling is characterized by the hopping matrix element Δ. The leads attached to the dots are modelled by ideal Fermi gases,

$$H_{\text{leads}} = \sum_{\ell=\text{L,R}} \sum_q \epsilon_q c_{\ell q}^\dagger c_{\ell q}, \tag{3}$$

where $c_{\ell q}^\dagger$ ($c_{\ell q}$) creates (annihilates) an electron with energy ϵ_q in lead $\ell = \text{L, R}$. As an initial condition, we employ the grand-canonical ensemble of the electrons in the leads at inverse temperature $\beta = 1/k_B T$ and with electrochemical potentials $\mu_{L/R}$. Therefore, the lead electrons are described by the equilibrium Fermi function $f_\ell(\epsilon_q) = \{1 + \exp[-\beta(\epsilon_q - \mu_\ell)]\}^{-1}$. For the initial density matrix, we then have

$$\rho_{\text{leads,eq}} \propto \exp\left[-\beta(H_{\text{leads}} - \mu_L N_L - \mu_R N_R)\right], \tag{4}$$

where $N_\ell = \sum_q c_{\ell q}^\dagger c_{\ell q}$ denotes the electron number in the left and right lead, respectively. From this it follows that all expectation values of the lead operators can be traced back to the expression $\langle c_{\ell' q'}^\dagger c_{\ell q}\rangle = \delta_{\ell\ell'}\delta_{qq'} f_\ell(\epsilon_q)$. The two dots couple via the tunnelling matrix element $V_{\ell q}$ to the state $|\ell q\rangle$ in the respective lead. The Hamiltonian describing this interaction has the form

$$H_{\text{dot-lead}} = \sum_q (V_{Lq} c_{Lq}^\dagger c_1 + V_{Rq} c_{Rq}^\dagger c_2) + \text{H.c.} \tag{5}$$

It will turn out that the influence of the tunnelling matrix elements is completely characterized by the spectral density $\Gamma_\ell(\epsilon) = 2\pi \sum_q |V_{\ell q}|^2 \delta(\epsilon - \epsilon_q)$ which becomes a continuous function of ϵ if the lead modes are dense. If all relevant lead states are located in the centre of the conduction band, the energy dependence of the spectral densities is not relevant and can be replaced by a constant, $\Gamma_{L/R}(\epsilon) = \Gamma_{L/R}$. This defines the so-called wide-band limit.

3.2. Master equation approach

The computation of stationary currents can be achieved by deriving a master equation for the dynamics of the dot electrons. Thereby, the central idea is to consider the contact Hamiltonian (5) as a perturbation. From the Liouville–von Neumann equation $i\hbar\dot{\rho} = [H, \rho]$ for the total density operator ρ one obtains by standard techniques [18] the approximate equation of motion

$$\dot{\rho}(t) = -\frac{i}{\hbar}[H_{\text{dots}}(t) + H_{\text{leads}}, \rho(t)] - \frac{1}{\hbar^2}\int_0^\infty d\tau [H_{\text{dot-lead}}, [\widetilde{H}_{\text{dot-lead}}(-\tau), \rho(t)]]. \tag{6}$$

The tilde denotes operators in the interaction picture with respect to the central system and the lead Hamiltonian, $\widetilde{X}(t) = U_0^\dagger(t)\, X\, U_0(t)$, where U_0 is the propagator without the coupling. The stationary current defined as the net (incoming minus outgoing) electrical current through contact ℓ is given by minus the time-derivative of the electron number in that lead multiplied by the electron charge $-e$, $I_L(t) = e(d/dt)\langle N_\ell\rangle$. From the master equation (6) it follows that

$$I_L(t) = e\,\text{tr}[\dot{\rho}(t) N_L] = -\frac{e}{\hbar^2}\int_0^\infty d\tau \left\langle [\widetilde{H}_{\text{dot-lead}}(-\tau), [H_{\text{dot-lead}}, N_L]]\right\rangle. \tag{7}$$

In the following, we specify the master equation (6) and the current formula (7) for studying two limiting cases: the first limit $U = 0$ describes non-interacting electrons. The second limit refers to strong Coulomb repulsion such that U is much larger than any other energy scale of the problem. Then, only the states with at most one excess electron on the wire are relevant.

3.2.1. Non-interacting electrons. In general, the relation between the states $|\phi_\alpha\rangle$ and the many-particle Hamiltonian (1) is established via the Slater determinant. Alternatively, one can resort to Green's functions. In the present case, knowledge of the Green's function at time $t = 0$ is already sufficient. Apart from a prefactor, it is given by the expectation value $P_{\alpha\beta} = \langle c_\beta^\dagger c_\alpha\rangle$ for which one obtains from equation (7) for the stationary current the expression

$$I_0 = \frac{e\Gamma_\ell}{\hbar}\sum_\alpha\Big[\sum_\beta \langle\phi_\beta|n_\ell\rangle\langle n_\ell|\phi_\alpha\rangle P_{\alpha\beta} - |\langle n_\ell|\phi_\alpha\rangle|^2 f_\ell(\epsilon_\alpha)\Big], \tag{8}$$

where the index 0 refers to $U = 0$. It can be shown that the current is independent of the index ℓ, i.e. independent of the contact at which it is evaluated. This reflects for a two-probe setting the validity of the continuity equation. For the

steady state expectation values $P_{\alpha\beta}$, we obtain from the master equation (6) the condition

$$\mathrm{i}(\epsilon_\alpha - \epsilon_\beta) P_{\alpha\beta} = \sum_{\ell=\mathrm{L,R}} \frac{\Gamma_\ell}{2} \Big\{ \langle\phi_\alpha|n_\ell\rangle\langle n_\ell|\phi_\beta\rangle \left[f_\ell(\epsilon_\alpha) + f_\ell(\epsilon_\beta) \right] - \sum_{\alpha'} \langle\phi_\alpha|n_\ell\rangle\langle n_\ell|\phi_{\alpha'}\rangle\, P_{\alpha'\beta} - \sum_{\beta'} \langle\phi_{\beta'}|n_\ell\rangle\langle n_\ell|\phi_\beta\rangle\, P_{\alpha\beta'} \Big\}. \tag{9}$$

In a non-equilibrium situation, the solution of this set of equations generally possesses non-vanishing off-diagonal elements, which in some cases turn out to be crucial.

3.2.2. Strong Coulomb repulsion. In the limit of strong Coulomb repulsion, U is assumed to be so large that at most one excess electron resides on the system. Thus, the available Hilbert space is restricted to the states $\{|0\rangle, c_\alpha^\dagger|0\rangle\}_{\alpha=1,2}$, such that the density operator can be written as

$$\rho = |0\rangle\rho_{00}\langle 0| + \sum_\alpha \left(c_\alpha^\dagger|0\rangle\rho_{\alpha 0}\langle 0| + |0\rangle\rho_{0\alpha}\langle 0|c_\alpha \right) + \sum_{\alpha\beta} c_\alpha^\dagger|0\rangle\rho_{\alpha\beta}\langle 0|c_\beta. \tag{10}$$

while the current expectation value (7) becomes

$$I_\infty = e\Gamma_\ell \sum_\alpha \Big[\sum_\beta \langle\phi_\beta|n_\ell\rangle\langle n_\ell|\phi_\alpha\rangle\, \bar{f}_\ell(\epsilon_\alpha)\rho_{\alpha\beta} - |\langle\phi_\alpha|n_\ell\rangle|^2 f_\ell(\epsilon_\alpha)\rho_{00} \Big], \tag{11}$$

where $\bar{f} = 1 - f$. The decomposition of the master equation (6) into the single-particle states $c_\alpha^\dagger|0\rangle$ provides for the stationary state the set of equations

$$\mathrm{i}(\epsilon_\alpha - \epsilon_\beta)\rho_{\alpha\beta} = \sum_{\ell=\mathrm{L,R}} \frac{\Gamma_\ell}{2} \Big\{ \langle\phi_\alpha|n_\ell\rangle\langle n_\ell|\phi_\beta\rangle \big(f_\ell(\epsilon_\alpha) + f_\ell(\epsilon_\beta) \big)\rho_{00} - \sum_{\alpha'} \langle\phi_\alpha|n_\ell\rangle\langle n_\ell|\phi_{\alpha'}\rangle\, \bar{f}_\ell(\epsilon_{\alpha'})\rho_{\alpha'\beta} - \sum_{\beta'} \langle\phi_{\beta'}|n_\ell\rangle\langle n_\ell|\phi_\beta\rangle\, \bar{f}_\ell(\epsilon_{\beta'})\rho_{\alpha\beta'} \Big\}. \tag{12}$$

In order to fully determine the density operator, we need in addition an expression for ρ_{00} which can also be derived from the master equation. A more convenient alternative is provided by the normalization condition $\mathrm{tr}\,\rho = \rho_{00} + \sum_\alpha \rho_{\alpha\alpha} = 1$. For the sake of completeness, we remark that it follows from the master equation (6) that $\rho_{\alpha 0} = \rho_{0\alpha} = 0$ in the stationary state.

3.3. Comparison with experimental data

Before establishing a quantitative relation between our model and the experimental results, we discuss the transport properties of the double-dot model qualitatively. Thereby we reveal that both Coulomb repulsion and an orbital degree of freedom play a role in the behaviour of a fixed, not too small source–drain voltage while the gate voltage is changed. For very large negative values of V_{gate}, the eigenstates of the double dot lie well above the chemical potential of both leads, and thus outside the voltage window. This means that lead states being in resonance with the dot states remain unoccupied, such that electron transport can only occur via co-tunnelling processes. Thus, the current will be rather small. When V_{gate} becomes larger such that the lower dot level lies within the voltage window (see figure 6(a)), resonant transport becomes possible, yielding a noticeable current. Increasing the voltage further, such that the second level also enters the voltage window, opens a second path for non-interacting electrons through the dots. In the case of strong Coulomb repulsion, however, double occupation of the dot is impossible and, thus, the second orbital cannot fully contribute to the transport. Accordingly, the increase of the current is smaller.

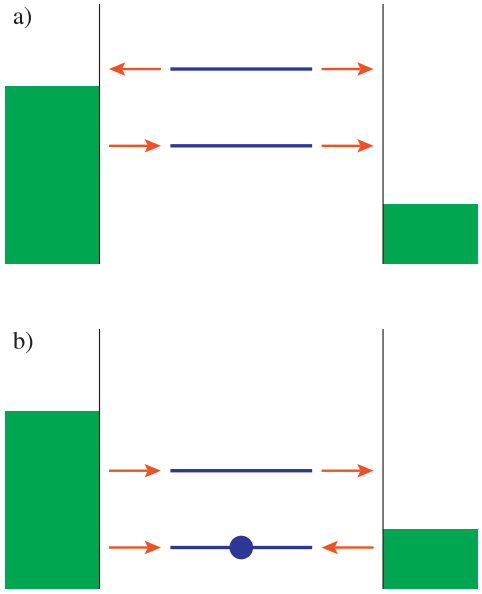

Figure 6. Sketch of the transport through eigen energy levels for different gate voltages. The arrows indicate the possible tunnel events for electrons into and out of the system. In panel (a), V_{gate} is so large that only one level lies within the voltage window, while the other one lies well above and is never occupied. Consequently, transport is interaction independent. If one level lies below both chemical potentials (b), it will be occupied in the steady state and, thus, strong Coulomb repulsion inhibits the electron transport.

The most significant difference between the two cases is found when only the upper level lies within the voltage window while the lower level is below both chemical potentials, as sketched in figure 6(b). Then the stationary state is characterized by an occupied lower level. Whether or not a further electron can enter and cause a non-vanishing current now depends on the strength of the Coulomb repulsion—for strong repulsion, transport is Coulomb blocked. Consequently, for the two limits under investigation, we obtain a current only in one of non-interacting electrons. This is visible as an even qualitative difference in the Coulomb diamond structure of figure 3: the scenario for non-interacting electrons complies with particle–hole symmetry. This has the consequence that the corresponding Coulomb diamond (figure 3(c)) is invariant under changing the sign of both the source–drain voltage and the gate voltage. For strong Coulomb repulsion, in contrast, the symmetry concerning the sign of V_{gate} is no longer present (see figure 3(b)). In particular for $V_{\mathrm{SD}} \approx 0$, the experimental data exhibit only one spot with high conductance, which is in clear contrast to the theoretical result for the non-interacting case shown in figure 3(c).

The limits of strong and zero interaction have in common that when the two energy levels enter the voltage window from above, the current increases in two steps whose separation is determined by the energy splitting δE of the two levels, i.e. they are separated by the voltage $\delta E/e$. This enables one to determine the excitation energy of an orbital degree of freedom by conductance measurements. Moreover, the source–drain voltage relates to the steepness of the triangle. Figure 4 shows again the measurement of figure 3(a) but now with the idealized diamond structure marked by dashed lines.

For a more quantitative treatment, we compare the structure of the experimental result in figure 3(a) with the theoretical Coulomb diamond in figure 3(b). This allows one to read off the tunnel coupling $\Delta = 0.8$ meV. For the slightly asymmetric lead–dot couplings $\Gamma_L = 0.2\Delta$ and $\Gamma_R = 0.25\Delta$, we obtain at the plateaus for the current the values 2.2 nA and 2.4 nA, respectively, which is of the order of the measured values at the edges of the Coulomb diamonds (2–3 nA).

The quantitative agreement between the experiment and the theoretical result for $U = \infty$ suggests that electrons in the relevant localized states of our sample strongly repel each other. This raises the question of which part of the sample (see figure 1) the localized states are formed in. The sawtooth pattern has been created by the chemical wet-etching, and four narrow constrictions intersect the long wire into three separate regions. In figure 2, features of a 1D system have been detected for less negative side gate voltages as discussed in an earlier section. This means that one of the narrower constrictions must govern the conduction process in the open channel regime, because it is unlikely that all constrictions represent identical tunnel barriers. However, we cannot identify which constriction dominates. Moreover, in samples like the one used in this work, randomly distributed charged impurities from the doping process are present. They can strongly influence the potential profile depending on their position during the cooling down process [19].

Unfortunately, without further investigation, we are not able to determine in which part of the sample the relevant levels are localized. With the data from the theoretical model for strong inter-dot coupling we nevertheless can infer that both dots must be rather close. Taking the curved shape of the etched potential into account, an unintentionally emerged dot is very likely as well.

4. Conclusion

We have studied Coulomb oscillations on lateral fabricated QDs near the pinch-off. In order to gain a theoretical understanding, we investigated a two-site model which implies the consideration of one orbital excitation. A comparison of the measured Coulomb diamond with theoretical predictions indicates that both Coulomb repulsion and orbital degrees of freedom play a significant role in the transport. The importance of Coulomb repulsion is emphasized by the fact that the corresponding model with non-interacting electrons makes qualitatively wrong predictions. Moreover, the theoretical results allow us to gauge the gate voltage and to determine the energy splitting associated with the orbital excitation. As a drawback, the measurement does not yield any conclusion about the nature and the location of the two relevant states. Studying a sample in which more orbital degrees of freedom play a dominant role might provide additional information. Such experiments should be accompanied by theoretical studies of finite Coulomb repulsion strength.

Acknowledgments

Financial support of the German Excellence Initiative via the 'Nanosystems Initiative Munich (NIM)' and of the Elite Network of Bavaria via the International Doctorate Programme 'NanoBioTechnology' is gratefully acknowledged. This work was supported in part by the Deutsche Forschungsgemeinschaft under contract number EB 365/5.

References

[1] Hayashi T, Fujisawa T, Cheong H D, Jeong Y H and Hirayama Y 2003 *Phys. Rev. Lett.* **91** 226804
[2] van der Wiel W G, De Franceschi S, Elzerman J M, Fujisawa T, Tarucha S and Kouwenhoven L P 2003 *Rev. Mod. Phys.* **75** 1
[3] Platero G and Aguado R 2004 *Phys. Rep.* **395** 1
[4] Kohler S, Lehmann J and Hänggi P 2005 *Phys. Rep.* **406** 379
[5] Davies J 1998 *The Physics of Low-Dimensional Semiconductors: An Introduction* 3rd edn (Cambridge: Cambridge University Press)
[6] Smith C 1996 *Rep. Prog. Phys.* **59** 235
[7] Fowler A, Hartstein A and Webb R 1982 *Phys. Rev. Lett.* **48** 196
[8] Pepper M 1978 *Phil. Mag.* B **37** 83
[9] Landauer R 1957 *IBM J. Res. Dev.* **1** 223
[10] Beenakker C and van Houten H 1991 *Solid State Phys.* **44** 1
[11] van Houten H, Beenakker C and Staring A 1992 *Single-Electron Tunneling and Mesoscopic Devices* (*Springer Series in Electronics and Photonics* vol 31) ed H Koch and H Lübbig (Berlin: Springer) pp 159–70
[12] Livermore C, Crouch C H, Westervelt R M, Campman K L and Gossard A C 1996 *Science* **274** 1332
[13] Ciorga M, Sachrajda A S, Hawrylak P, Gould C, Zawadzki P, Jullian S, Feng Y and Wasilewski Z 2000 *Phys. Rev.* B **61** R16315
[14] Kouwenhoven L P 1995 *Science* **268** 1440
[15] Weis J 2003 *Fundamentals of Nanoelectronics—Lecture Manuscripts of the 34th Spring School of the Department of Solid State Research* (*Matter and Materials* vol 14) ed S Blügel, M Luysberg, K Urban and R Waser (Jülich: Forschungszentrum Jülich GmbH) chapter D6, pp D6.1–D6.33
[16] Novotný T 2002 *Europhys. Lett.* **59** 648
[17] Kaiser F J, Strass M, Kohler S and Hänggi P 2006 *Chem. Phys.* **322** 193
[18] May V and Kühn O 2003 *Charge and Energy Transfer Dynamics in Molecular Systems* 2nd edn (Weinheim: Wiley–VCH)
[19] Nicholls J, Frost J, Ritchie D, Grimshaw M and Jones G 1993 *Phys. Rev.* B **48** 8866